

# Automated Microscopy and Machine Learning for Expert-Level Malaria Field Diagnosis

Charles B. Delahunt

Global Good/Intellectual Ventures Laboratory  
Bellevue, Washington, USA  
University of Washington, Seattle, Washington, USA

Couros Meharian, Liming Hu, Shawn K. McGuire,  
Cary R. Champlin, Matthew P. Horning,  
Benjamin K. Wilson

Global Good/Intellectual Ventures Laboratory  
Bellevue, Washington, USA

Clay M. Thompon

Creative Creek Software  
Camano Island, Washington, USA

**Abstract**—The optical microscope is one of the most widely used tools for diagnosing infectious diseases in the developing world. Due to its reliance on trained microscopists, field microscopy often suffers from poor sensitivity, specificity, and reproducibility. The goal of this work, called the Autoscope, is a low-cost automated digital microscope coupled with a set of computer vision and classification algorithms, which can accurately diagnose a variety of infectious diseases, targeting use-cases in the developing world. Our initial target is malaria, because of the high difficulty of the task and because manual microscopy is currently a central but highly imperfect tool for malaria work in the field. In addition to diagnosis, the algorithm performs species identification and quantitation of parasite load, parameters which are critical in many field applications but which are not effectively determined by rapid diagnostic tests (RDTs).

We have built a hardware prototype which can scan approximately 0.1  $\mu\text{L}$  of blood volume in a standard Giemsa-stained thick smear blood slide in approximately 20 minutes. We have also developed a comprehensive machine learning framework, leveraging computer vision and machine learning techniques including support vector machines (SVMs) and convolutional neural networks (CNNs). The Autoscope has undergone successful initial field testing for malaria diagnosis in Thailand.

**Keywords**—malaria; microscopy; computer-aided diagnosis; computer vision; machine learning.

## I. INTRODUCTION

The optical microscope is one of the most widely used tools for diagnosing infectious diseases in the developing world [1][2]. There are several reasons for this including its low cost per test, the general availability of microscope hardware, and its ability to diagnose a variety of diseases. Some common diseases diagnosed with microscopes in low-resource settings include malaria, tuberculosis, different forms of trypanosomiasis, Borrelia infection, and helminth infection. Despite these advantages, field microscopy often suffers from poor sensitivity, specificity, and reproducibility. This is due to

its reliance on trained microscopists to interpret what is seen through the microscope. While quality assurance and assessment exist in many areas for microscopy, these face many limitations including a shortage of trained experts [3].

In this work, we present a low-cost automated digital microscope called the Autoscope. In addition to automated image acquisition, the Autoscope is coupled to a set of computer vision and classification algorithms, which can accurately diagnose a variety of infectious diseases, targeting use cases in the developing world. The goal of Autoscope is to provide expert level microscopy with a user interface that is operable by a healthcare worker with an average level of training.

Our initial target and the subject of this work is malaria diagnosis. We chose malaria as an initial target for several reasons. First, malaria remains a significant burden on global health, with an estimated 580,000 deaths per year [5]. Accurate diagnosis of malaria is an important part of case management. Secondly, manual microscopy for malaria is currently a central but highly imperfect tool in the field [5]–[6]. It is likely to retain a central role for years to come. Microscopy can perform species identification and quantitation of parasite load, parameters that are critical in many field applications but which are not effectively determined by rapid diagnostic tests (RDTs). Lastly, expert level microscopy for malaria is a highly difficult task because of the fine resolution required of the microscope hardware and the subtle features that must be correctly interpreted to accurately diagnose the disease while distinguishing between the five pathogenic species in humans [15]. By proving Autoscope’s capabilities on this task, we will demonstrate the ability of a machine to perform one of the hardest tasks today performed by field microscopists.

In this work, we describe some of the technical specifications of the Autoscope and its accompanying computer vision algorithms, as well as describe the system we have developed for training and testing the algorithms. We present data and results from a World Health Organization (WHO) 55 reference slide set and from a preliminary field test in Thailand and discuss future work for the project.

---

Research sponsored by the Global Good Fund.

## II. MATERIALS AND METHODS

### A. Datasets

The goal of Autoscope is to diagnose malaria using Giemsa-stained blood samples from the field (with the high variability in quality that field conditions imply), achieving a limit of detection (LoD)  $< 50$  parasites/ $\mu\text{L}$  (i.e. 1 parasite/1E5 red blood cells), in fully automated fashion. While thin smears are generally easier to analyze than thick smears due to clearer morphological information, thin smears from the field are unreliable in quality and their total usable blood volume is insufficient to attain a 50 p/ $\mu\text{L}$  LoD. Thus, thin smears are not practical for diagnosis of field samples, so the Autoscope uses thick smears for diagnosis.

The training data consisted of Giemsa-stained blood samples, both *Plasmodium falciparum*-positive and uninfected, from 7 locations worldwide (see Fig. 1). Our goal was to maximize variety, since field slides vary tremendously in quality, color (e.g. from stain pH), and type of artifacts. In addition, *falciparum* parasites exhibit distinct morphologies at different stages of growth. We wished to capture this diversity as well. The modules of the algorithm described in this paper target *P. falciparum*, in thick smears only.

### B. Hardware

The Autoscope hardware shown in Fig. 1 consists of a small aluminum chassis approximately 37 cm in height with a width and depth of 17 cm and 19 cm respectively. The small footprint allows for carry-on travel of the device while also minimizing space requirements on a lab benchtop. See 0. The initial Autoscope prototype described herein was designed to withstand ambient temperature ranges of  $5^\circ$  to  $35^\circ$  C and at 100% humidity. However, extended testing at the extreme ends of this spectrum have not been performed. Maintenance of the device consists of cleaning the microscope objective in the same manner as a manual microscope. Power consumption of the device during scan is  $\sim 15.8$  W. This does not count laptop power consumption. The Autoscope final cost will likely be between \$1500 and \$4000, roughly 1x to 3x the cost of a standard lab microscope. Use of the Autoscope does not require special skills (although repair would likely not be possible by field clinic staff). The Autoscope requires blood slides prepared and stained according to current protocols for manual microscopists diagnosing malaria via Giemsa stained blood slides.

In order to satisfy the low limit of detection requirements, the Autoscope must scan at least  $0.1 \mu\text{L}$  of blood, which results in 300 fields-of-view (FOV) given the image size produced by the camera and the field size of the objective. Given the small size of malaria parasites, a  $100\times$  1.25 NA oil immersion microscope objective is used to adequately resolve features of interest inherent in the parasites for proper identification and classification. This results in a small depth of field of approximately  $0.6 \mu\text{m}$ , which leads to the requirement that parasites be within approximately  $0.3 \mu\text{m}$  of the ideal focal depth. To this end, a linear piezo motor (shown in Fig. 1) accompanied by an optical (linear) encoder was used to provide rapid motion along the z-axis with a resolution of  $\pm 0.1 \mu\text{m}$ . Focus performance was determined using a Brenner

gradient algorithm across the FOV resulting in a focus score for each z-stack level. The score is then used in a Fibonacci search algorithm to expedite location of optimal focal depth. Parasites in a given FOV are often located at different depths and so nine images differing by  $0.3 \mu\text{m}$  in height are taken for each FOV to ensure an in-focus image of every parasite is captured. A 1.0 Watt white LED combined with a diffuser results in an exposure time of 8-20 ms, depending on the malaria sample being examined. This results in an overall scan time of approximately 20 minutes with approximately  $0.1 \mu\text{L}$  of blood being examined.

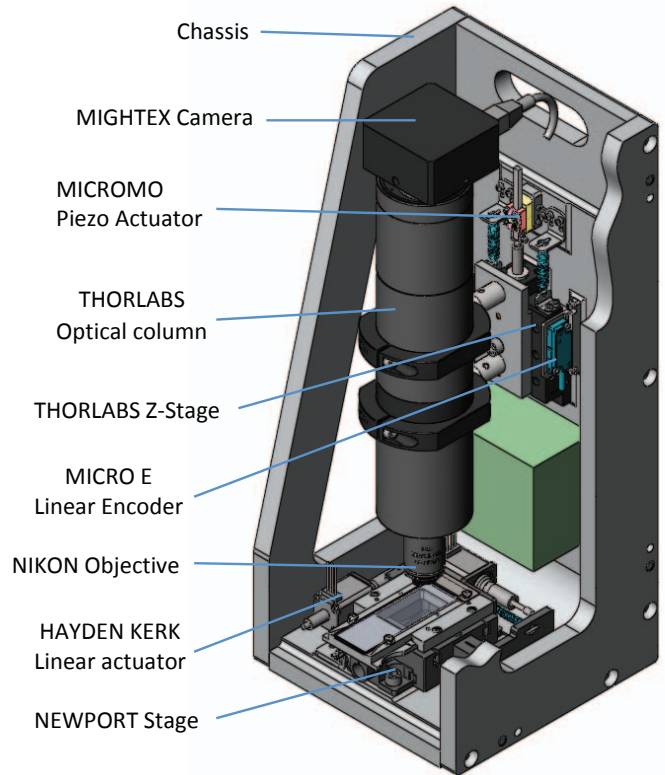


Fig. 1. 3D Model of Autoscope chassis

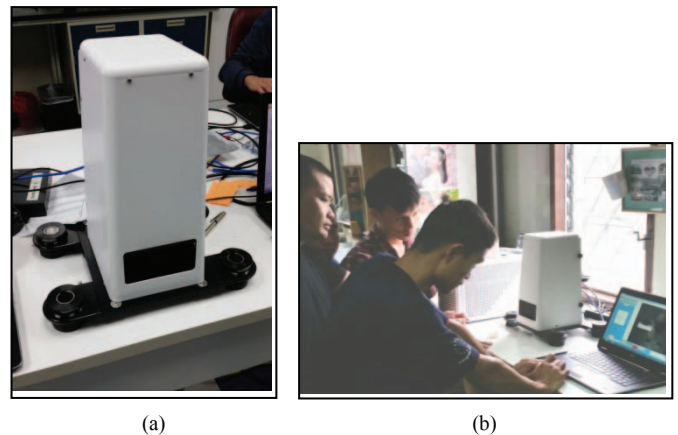


Fig. 2. Autoscope (a) on lab bench, (b) in the field at SMRU

TABLE I. LIST OF SLIDES, NEGATIVES AND *FALCIPARUM* ONLY

Source	# Negatives	# falciparum	Parasitemia (p/ $\mu$ L)
SMRU <sup>a</sup>	50	33	5,000–150,000
UPCH <sup>b</sup>	50	0	N/A
RITM <sup>c</sup>	40	3	500–1,500
HTD <sup>d</sup>	1	8	500–4,000
ACMED <sup>e</sup>	1	5	350–141,000
AMREF <sup>f</sup>	1	16	500–300,000
KEMRI <sup>g</sup>	20	10	100–200
RITM <sup>h</sup>	20	23	100–2,000

<sup>a</sup> Shoklo Malaria Research Unit, Thailand

<sup>b</sup> Universidad Peruana Cayetano Heredia, Peru

<sup>c</sup> Research Institute of Tropical Medicine, Philippines

<sup>d</sup> London Hospital of Tropical Diseases, UK

<sup>e</sup> Andri Centre of Excellence for Malaria Diagnosis, Nigeria

<sup>f</sup> African Medical and Research Foundation, Kenya

<sup>g</sup> Kenya Medical Research Institute, Kenya

<sup>h</sup> World Health Organization (WHO) dataset from RITM

### C. Annotation

Image sets were manually annotated using a variety of software applications having a graphical user interface (GUI). Annotations of parasites were cross-checked by multiple on-site and off-site experts. Negative samples were assumed to be parasite-free, since they were PCR-negative. All annotated objects, as well as sample meta-data, were stored in an SQL database. Manual annotation recorded only the x-y location of each parasite; best focus z-stack level was computed by the algorithm.

An example of a portion of a field-of-view image is shown in Fig. 3a. Two white blood cells can be seen in the image, as well as three early-stage *P. falciparum* trophozoites which are indicated with a red plus sign. Fig. 3b shows a close up of the *P. falciparum* ring closest to the center of the image. The nucleus is a dark, round blob that is typically purple in color, although the color can vary between blue, violet, and purple depending on the imaging characteristics and the Giemsa stain pH. The cytoplasm is a somewhat less dark, thin blob that is spatially associated with the nucleus (or nuclei). The color is typically blue and the shape highly variable. For example, *P. falciparum* trophozoites can look like a semicolon or a basket as well as a variety of other shapes. In some instances, trophozoites with two nuclei can take on a characteristic headphone shape (not shown).

Another typical characteristic of these images is that they contain artifacts (distractors) that share many of the same image features as *P. falciparum* rings. To the untrained eye, they can look like parasites, and one of the main challenges of Autoscope was to distinguish between real parasites and distractors. Application of the Autoscope diagnostic algorithms to non-malarial diseases in 2016 will provide datasets for pathogens that might act as distractors for malaria (e.g. babesia).

### D. Image Analysis

The annotated images provide the ground truth for the Autoscope machine learning system. The image analysis framework is structured as a classical computer vision architecture. The system consists of the following modules:

#### 1. Preprocessing

There can be considerable color variability between images. Even images captured with the same Autoscope device can vary in color based on the pH of the Giemsa stain as mentioned above. These color differences are not germane to discriminating between parasites and distractors. The preprocessing module transforms the scanned color images to take on a consistent appearance.

#### 2. Detection

The detection module finds parasite candidate objects in all the field-of-view images acquired from a blood sample. A fast, coarse level of classification is employed to detect these candidate locations. Subsequent to the detection stage, only candidate object locations are examined.

The ground truth is leveraged to train the Autoscope machine learning algorithms by establishing a correspondence between the detected objects and the annotated parasites. A detected object that coincides with an annotated parasite is used as a positive sample to train the machine learning algorithm. Annotated parasites that are not detected are also used as positive training samples. Detected objects that do not correspond to any annotated parasite are used as negative training samples (distractors). The output of the correspondence algorithm is a set of objects that are labeled as either parasites or distractors.

#### 3. Segmentation

The segmentation module automatically delineates the nucleus and the cytoplasm blobs at candidate object locations. This segmentation is performed on positive and negative samples alike, mimicking what would be done in a field trial where the ground truth is unknown. The nucleus and cytoplasm are the cornerstone for many of the extracted features that are the basis of the classification algorithms.

#### 4. Feature extraction

Two feature extraction approaches have been adopted in Autoscope: traditional feature engineering as well as convolutional neural networks. The traditional features can be divided into four major groupings. Morphological features capture shaped-based attributes that characterize the nucleus and cytoplasm. Color features characterize the observed color differences between the nucleus and cytoplasm. Texture features help to distinguish between distractors which are rich in texture from *P. falciparum* rings which are essentially simple objects without texture. Finally, a range of rectangular Haar features provide a numerical representation of the spatial relationship between nucleus and cytoplasm.



## 5. Classification

In the training phase, the labeled objects are used to train a classifier based on their computed features. A number of different classifiers have been employed in the classification module, including a linear support vector machine (SVM), a radial basis function SVM (we used the `libsvm` package [16]), a conventional neural network (NN), as well as a Gradient-Boosted Decision Tree (GBM). A two-stage classifier (linear SVM followed by NN) gave the best results. It should be noted that the hyperparameters of the classifiers (e.g. C value for a linear SVM) are tuned on a validation set, and subsequently applied to testing sets. The classifiers output a classifier score in the range  $[0,1]$ , which approximates the probability that a candidate object is a parasite.

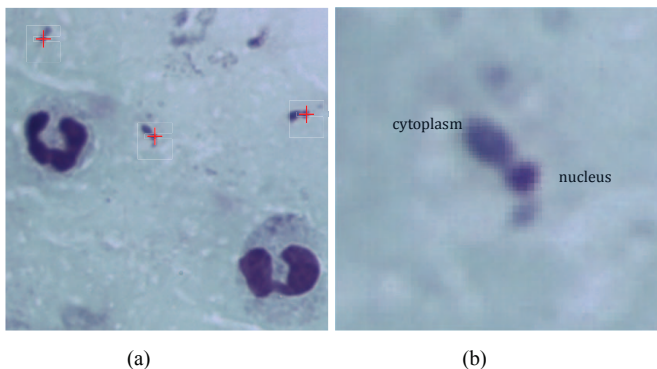


Fig. 3. (a) Autoscope FOV image, (b) close-up of *P. falciparum*

## 6. Diagnosis

In validation and testing phases, the diagnosis module makes a determination whether a blood sample has malaria or not. The determination is based on the classifier scores for all of the detected candidate objects. The algorithm counts the number of objects above an object-level classifier score threshold ( $\rho$ ). The algorithm then applies a second threshold ( $\theta$ ) on the number of objects above the classifier threshold  $\rho$ .

In addition to making a determination of whether a blood sample is infected, the Autoscope software framework computes an estimate of the parasitemia, which is defined as the number of parasites per 8,000 white blood cells. This is a standard proxy for parasites per microliter ( $\text{p}/\mu\text{L}$ ), used when the blood volume is not directly observable.

Fig. 5 shows block diagrams for the process flow in the training, validation, and testing phases of the Autoscope software framework. It is apparent from the figures that the preprocessing, detection, segmentation, and feature extraction phases are common to all three modes of operation. Object-level ground truth annotation is a requirement for the training and validation sets. In the validation and testing phases, the classifier is operated in prediction mode: training does not occur. Validation results are used to tune the classifier hyperparameters, and to tune the diagnosis thresholds. Feature selection is optionally used to trim the features down to a

minimal discriminatory set. For the testing phase, object-level annotation is optional. With ground truth annotation, it is possible to report object-level ROC and Precision-Recall curves for the testing set. Without it, sample-level sensitivity, specificity, and parasitemia accuracy may be reported.

In the field, the algorithm outputs diagnosis and quantitation information, and thumbnails of high-scoring objects (i.e. possible parasites) for inspection by the human user. In addition, it saves all the images, and a file with each object's location, feature, and scoring information.

## III. RESULTS

### A. WHO55 diagnosis

The algorithm was trained on 27 *P. falciparum*-positive samples (50 FOVs each, several thousand parasites), and 36 negative samples (50 FOVs each), drawn from all the collections listed in Fig. 1 (except KEMRI and RITM WHO). The algorithm's diagnosis parameters were set by ensuring 90% sample-level specificity on a validation set of negative samples from RITM only.

The algorithm was then applied to a separate test set, consisting of the *P. falciparum* component of a WHO55 set (source: RITM) as well as 3 low-parasitemia samples from SMRU. This test set included 20 negative samples, 10 RITM *P. falciparum* samples (parasitemia in the range  $100 - 200 \text{ p}/\mu\text{L}$ ), and 14 RITM and SMRU *P. falciparum* samples ( $200 - 1200 \text{ p}/\mu\text{L}$ ). Fig. 6 shows typical suspected parasites detected by the algorithm. TABLE II. gives Autoscope diagnosis results. Autoscope sensitivity and specificity exceed the diagnosis requirements for a WHO Level 1 (expert) microscopist. The algorithm reported in TABLE II. did not incorporate CNN-derived features.

Fig. 4 shows a heat map of the balanced accuracy =  $0.5 * (\text{sensitivity} + \text{specificity})$ , over the 2-D space of  $\rho$  and  $\theta$ . Everything to the right of the diagonal black boundary gives  $\geq 90\%$  specificity on the validation set. This constraint was used to set the diagnosis parameters before testing the WHO set. The top left region has low accuracy on the WHO set due to low specificity. The bottom right region has low accuracy due to low sensitivity. The central region has accuracy  $\geq 90\%$ , and also obeys the validation set specificity constraint. Any parameter pair in this central region would meet Level 1 WHO accuracy requirements. There are other parameter regions to the left of the black diagonal boundary which give accuracy  $\geq 90\%$  on the WHO set, but these regions were rejected during tuning on the validation set.

### B. Thailand field test

As a hardware test, two Autoscoptes were deployed to SMRU clinics in Thailand during the malaria season Dec 2014 – Jan 2015. A total of 168 samples were collected and processed: 95 negatives, 8 *P. falciparum*, 62 *P. vivax*, and 3 mixed species.

A version of the algorithm was trained on 11 *P. falciparum*-positive samples (50 FOVs each, total thousands of parasites), and 25 negative samples (50 FOVs each), drawn

mainly from SMRU samples (excluding samples collected during the field test). The diagnosis thresholds were set by ensuring 90% sample-level specificity on a validation set of negative samples from SMRU only (excluding samples collected during the field test). The goal was to tailor training to the region where the Autoscope was being tested.

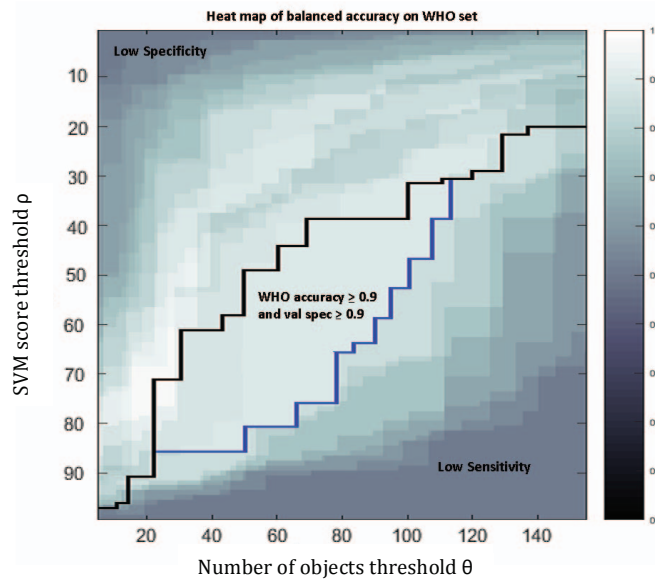


Fig. 4. Heatmap of Autoscope's balanced accuracy on the WHO set

Sample-level specificity on field data was 92%. Limit of Detection (LoD) on the few *P. falciparum* samples matched the results on the WHO55 set (LoD < 300 p/μL, limited by the parasitemia of available samples in the set). Although *P. vivax* parasites were entirely absent from the training set, the algorithm detected many *P. vivax* samples, with LoD on *P. vivax* ≈ 3000 p/μL. This sensitivity to *P. vivax* was due to detection of *P. vivax* ring stage parasites that sufficiently resembled *P. falciparum* ring stages to be captured by the algorithm. The percentage of early ring-stage forms in a given *P. vivax* infection can range from 0 to 100%. Thus the high LoD of the algorithm (compared to LoD on *P. falciparum*) reflects the fact that only a fraction of *P. vivax* parasites present as ring stage trophozoites.

The hardware performed smoothly in the field. One of the devices experienced sporadic trouble with camera connectivity. The algorithm software performed smoothly.

#### IV. DISCUSSION

The goal of Autoscope is to diagnose malaria using Giemsa-stained blood samples from the field with LoD < 50 p/μL, in fully automated fashion. Autoscope is, to our knowledge, the first fully automated hardware-software system to demonstrate WHO Level 1 diagnosis expertise on *P. falciparum* using field slides.

Because Autoscope uses Giemsa-stained field samples prepared according to current standard practice, it can be readily deployed to the field with minimal infrastructure changes. It targets the LoDs required by field use cases and it

can detect all species (in contrast to, for example, hemozoin-based methods that risk low sensitivity on *P. falciparum* [17]). Therefore, it can potentially make a substantial difference to known use cases such as patient case management.

The results presented here apply only to *P. falciparum*. Two algorithm modules remain: Diagnosis of non-*P. falciparum* species (*P. vivax*, *P. ovale*, and *P. malariae*) on thick smear; and species differentiation (e.g. between *P. vivax* and *P. ovale*) on thin smear. Non-*P. falciparum* species are easier to identify than *P. falciparum* due to the presence of larger late stage parasites. Thin smears are in general easier to analyze than thick smears, as stated above. Development continues on these two modules, as well as on improvements to the *P. falciparum* module, deeper exploration of convolutional neural network architectures, and improvements to the hardware (e.g. speed, cost).

To be maximally useful in the field, an Autoscope should also be able to diagnose other parasites (e.g. loa loa, Borrelia) and do basic hematology (differential). Since other parasites are orders of magnitude larger than malaria parasites, these are fundamentally easier tasks, and are targets for future work.

#### ACKNOWLEDGMENT

The authors gratefully acknowledge: Bill and Melinda Gates for their sponsorship through the Global Good Fund; David Bell for his guidance and support; Jane Carter, Peter Chiodini, Mehul Dhorda, Dionicia Gamboa, Ken Lilley, Earl Long, Stephane Proux, and Carol Sibley for serving on the technical advisory panel and generously sharing their expertise.

#### REFERENCES

- [1] Microscopy for the detection, identification and quantification of malaria parasites on stained thick and thin blood films in research settings. World Health Organization, May 2015.
- [2] Heidi Albert, Yukari Manabe, George Lukyamuzi, Patrick Ademun, Sheena Mukkada, Barnabas Nyesiga, Moses Joloba, C. N. Paramasivan, Mark D. Perkins, "Performance of three LED-based fluorescence microscopy systems for detection of tuberculosis in Uganda," PLoS ONE 2010, doi: 10.1371/journal.pone.0015206.
- [3] Sania Ashraf, Angie Kao, Cecilia Hugo, Eva M Christophel, Bayo Fatunmbi, Jennifer Luchavez, Ken Lilley, and David Bell "Developing standards for malaria microscopy: external competency assessment for malaria microscopists in the Asia-Pacific," Malaria Journal 2012, 11:352, doi:10.1186/1475-2875-11-352.
- [4] Moses Kiggundu, Samuel L. Nsobya, Moses R. Kanya, Scott Filler, Sussan Nasr, Grant Dorsey, and Adoke Yeka, "Evaluation of a comprehensive refresher training program in malaria microscopy covering four districts of Uganda," Am. J. Trop. Med. Hyg. 2011 vol. 84 no. 5, pp. 820-824, doi: 10.4269/ajtmh.2011.10-0597.
- [5] World Malaria Report 2014. World Health Organization, 2014.
- [6] Durrheim D N, Becker P J, Billingham K, "Diagnostic disagreement—the lessons learnt from malaria diagnosis in Mpumalanga," S. Afr. Med. J. 1997, 87:1016.
- [7] Kachur SP, Nicolas E, Jean-Francois V, Benitez A, Bloland PB, Saint Jean Y, Mount DL, Ruebush TK 2nd, Nguyen-Dinh P, "Prevalence of malaria parasitemia and accuracy of microscopic diagnosis in Haiti," October 1995. Rev Panam Salud Publica 1998, 3:35-39.
- [8] Kain KC, Harrington MA, Tennyson S, Keystone JS, "Imported malaria: prospective analysis of problems in diagnosis and management," Clin Infect Dis 1998, 27:142-149.
- [9] Kilian AH, Metzger WG, Mutschelknauss EJ, Kabagambe G, Langi P, Korte R, von Sonnenburg F, "Reliability of malaria microscopy in

epidemiological studies: results of quality control,” Trop Med Int Health 2000, 5:3-8.

- [10] Coleman RE, Maneechai N, Rachaphaew N, Kumpitak C, Miller RS, Soyseng V, Thimasarn K, Sattabongkot J, “Comparison of field and expert laboratory microscopy for active surveillance for asymptomatic *Plasmodium falciparum* and *Plasmodium vivax* in western Thailand,” Am J Trop Med Hyg 2002, 67:141-144.
- [11] O’Meara WP, McKenzie FE, Magill AJ, Forney JR, Permpanich B, Lucas C, Gasser RA Jr, Wongsrichanalai C, “Sources of variability in determining malaria parasite density by microscopy,” Am J Trop Med Hyg 2005, 73:593-598.
- [12] Kahama-Maró J, D’Acremont V, Mtasiwa D, Genton B, Lengeler C, “Low quality of routine microscopy for malaria at different levels of the health system in Dar es Salaam,” Malaria Journal 2011, 10:332.

- [13] Nankabirwa J, Zurovac D, Njogu JN, Rwakimari JB, Counihan H, Snow RW, Tibenderana JK, “Malaria misdiagnosis in Uganda-implications for policy change,” Malaria Journal 2009, 8:66.
- [14] Zurovac D, Midia B, Ochola SA, English M, Snow RW, “Microscopy and outpatient malaria case management among older children and adults in Kenya,” Trop Med Int Health 2006, 11:432-440.
- [15] Basic malaria microscopy – Part I: Learner’s guide. Second edition. World Health Organization, February 2010.
- [16] Chih-Chung Chang and Chih-Jen Lin, “LIBSVM: a library for support vector machines,” ACM Transactions on Intelligent Systems and Technology, 2:27:1--27:27, 2011. Software available at <http://www.csie.ntu.edu.tw/~cjlin/libsvm>.
- [17] Charles Delahunt, Matthew P Horning, Benjamin K Wilson, Joshua L Proctor and Michael C Hegg, “Limitations of haemozoin-based diagnosis of *Plasmodium falciparum* using dark-field microscopy,” Malaria Journal 2014, 13:147, doi:10.1186/1475-2875-13-147.

TABLE II. RESULTS OF AUTOSCOPE APPLIED TO THE *P. FALCIPARUM* PORTION OF A WHO55 SET. ROW 3 GIVES THE WHO REQUIREMENTS FOR LEVEL 1 (EXPERT) MICROSCOPISTS.

	# slides	Parasitemia (p/μL)	Sensitivity	Specificity	LoD (p/μL)
WHO set (RITM)	10 pos/20 neg	100 – 200	100%	95%	< 100
Other <i>P. falciparum</i>	14 pos	200 – 1,200	100%	95%	
Level 1 Reference	10 pos/20 neg	80 – 200	90%	90%	80

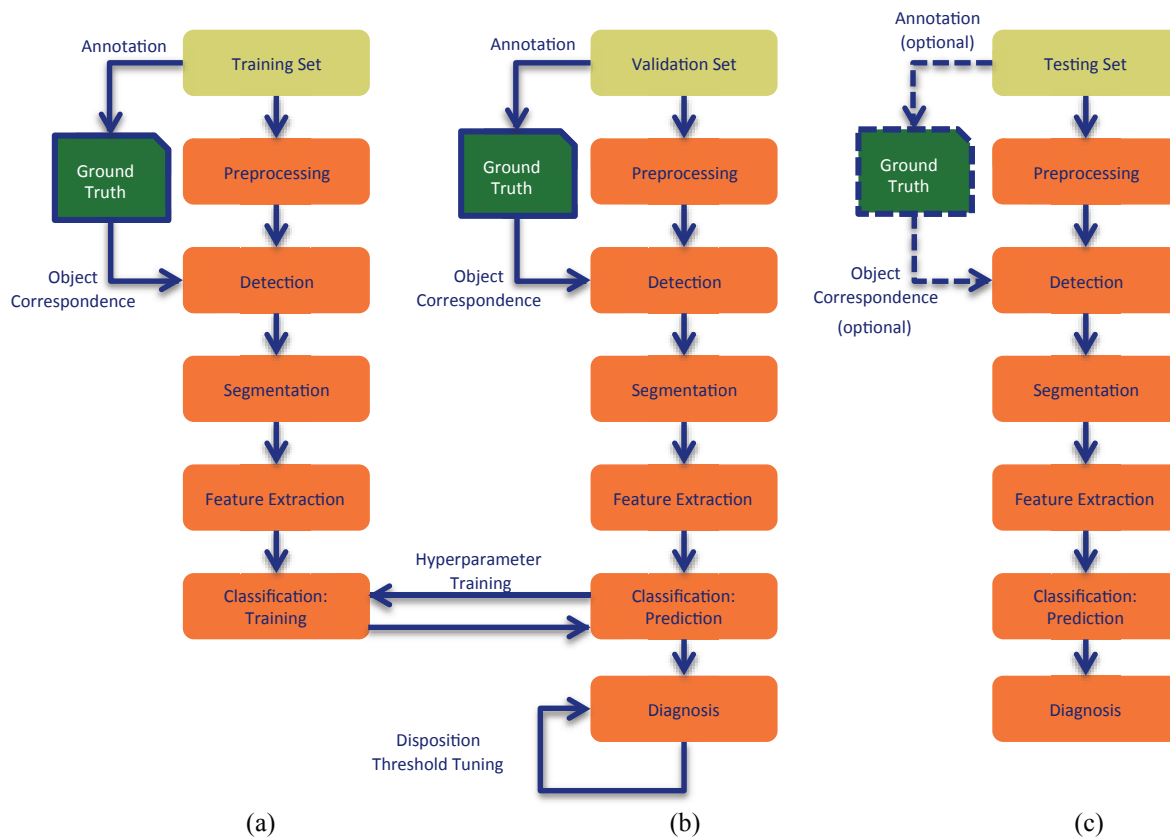


Fig. 5. Autoscope process flow in (a) training, (b) validation, and (c) testing phases

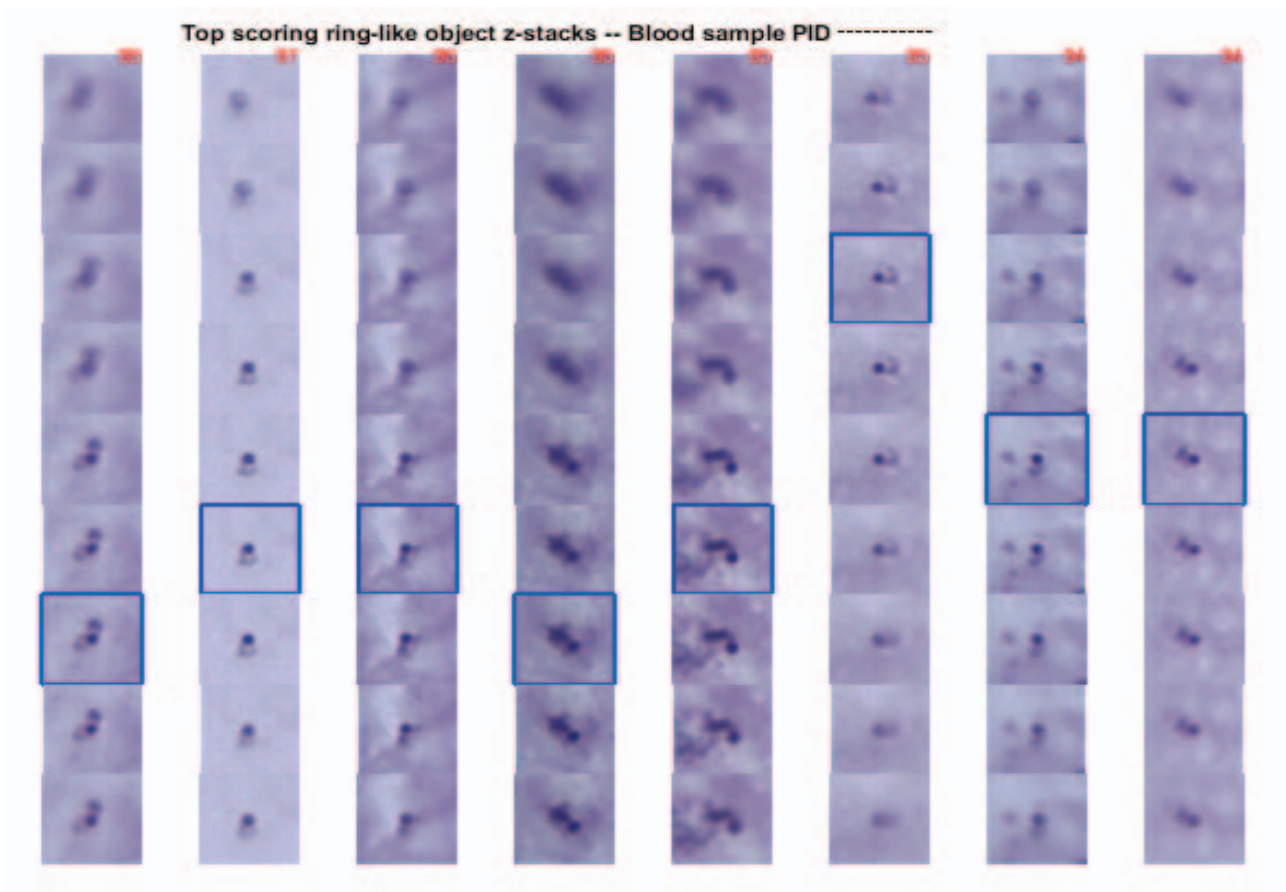


Fig. 6. Output of Autoscope algorithm showing z-stack thumbnails of top-scoring parasite suspects. The most in-focus thumbnail is framed in blue.